Dynamic Regulation of Proton and Water Transport through an Acylhydrazone-Based Photoresponsive Channel

Paras Wanjari, Ioan Stroia, Arie van der Lee, Marc Baaden, Mihail Barboiu

Dynamic Regulation of Proton and Water Transport Through Acylhydrazone Based Photo-responsive Channel

Paras Wanjari,[†] Ioan Stroia,[†] Arie van der Lee,[†] Marc Baaden[$] and Mihail Barboiu[†,*]

[†] Institut Européen des Membranes, Adaptive Supramolecular Nanosystems Group, University of Montpellier, ENSCM-CNRS, UMR5635, Place E. Bataillon CC047, 34095 Montpellier, France

[$] Université Paris Cité, CNRS, Laboratoire de Biochimie Théorique, 13 rue Pierre et Marie Curie, 75005, Paris, France

ABSTRACT: Proton transport is crucial for cellular energy, and synthetic systems having the ability to control this process offer promising applications in drug development and cancer treatment. Herein we report a unique light-responsive proton/water transport system using self-assembled acylhydrazone-imidazole channels with tunable activity *via E–Z* isomerization. Three channel-forming molecules with varying alkyl chain were synthesized namely **1a (C4)**, **1b (C8)** and **1c (C12)**. The photoswitching behaviour of the molecule was confirmed by UV-Vis spectroscopy within the liposome. The crystallographic analysis revealed that the *E*-isomer forms a H-bonded proton transport pathway mediated by water molecules. Patch clamp assays confirmed proton channel formation for **1a** with a transport rate of 2.18×10^7 H^+/s/channel and high proton selectivity over other ions. Ion transport assays with EYPC-LUVs entrapped with HPTS and NaCl revealed complete rejection of external cations and anions. The compounds demonstrated significant proton transport when combined with valinomycin, indicating transmembrane proton transport for **1a-c**. Upon irradiation at 310 nm, all derivatives showed increased proton transport rates, which subsequently decreased after exposure to 365 nm, confirming the photo-responsive behaviour of the system. A similar trend was observed in water transport, where the single-channel permeability of 1a increased from 6.5×10^6 to 3.5×10^7 water molecules/s/channel upon switching from the *E* to *Z* isomers, then decreased to 1.8×10^7 after reverting to the E conformer. Molecular simulation confirmed that stable supramolecular porous water crystal patches may form, featuring multivalent water H-bonding to acylhydrazone and imidazole units that serve as water-cluster relays within the channel.

INTRODUCTION

Transmembrane proteins are vital for cellular physiology, facilitating the regulated movement of ions across biological membranes[1]. These proteins play a critical role in pH homeostasis[2], signal transduction and energy production[3]. The precise regulation of ion flux across the cell membranes is essential for maintaining its volume, osmotic balance and the electrochemical gradients required for cellular processes. For instance, proton gradients across inner mitochondrial membranes are fundamental to ATP synthesis[4]. Dysfunctions in natural ion-channel proteins can severely disrupt cellular and systemic functions, leading to diseases such as Parkinson's[5], neonatal diabetes[6], neuropathic pain[7], cystic fibrosis[8], etc. Understanding the structural and functional mechanisms of ion channels is crucial for the diagnosis and treatment of related disorders, making them a prominent focus of biomedical research[9]. One emerging therapeutic approach involves the development of artificial ion channels designed to replace defective biological channels, thereby restoring normal ion transport. Additionally, these synthetic channels show promise in applications beyond therapeutic replacement, including anticancer and antibacterial activities by triggering cell apoptosis[10], underscoring their potential in diverse biomedical fields.While numerous synthetic channels for ions[11–14], water[15–19] and small molecules[20] have been developed, few exhibit selective proton transport across lipid bilayers[21,22]. Proton transport among all the other ions usually brings a higher level of difficulty owing to its smaller size and higher dehydration energy, requiring a precise control over protonation and deprotonation states to facilitate its translocation without disrupting other cellular functions.[23] Matrix-2 (M2) Influenza A virus proton channel has inspired artificial systems that mimic its proton transport mechanism[24]. The channels primarily rely on proton hopping *via* water wires,[25,26] a process known as the Grotthuss mechanism[27]. An alternative strategy involves proton relay through N-H chains within a helical unimolecular proton channel[28]. Molecular dynamics simulations have revealed that acetic acid can act as a molecular rotor, coordinating water arrays to facilitate proton transport[29]. Our group has previously reported the well-known I-quartet-[30] or saccharide rim-appended pillar[5]arene[22] artificial water channels, which facilitate water transport through the formation of a continuous water wires/clusters and enable proton transport *via* the Grotthuss mechanism. In addition to well-defined structural pathways, some systems can transport protons through undefined or dynamic routes, yet still achieve efficiency comparable to natural proton channels.[31]

Despite these successes, these artificial systems lack spatiotemporal control, which limits their control over the transport of ions thus becoming a hinderance for their usage in biological systems. To address this challenge, researchers have investigated stimuli-responsive systems in various ion transporters, including Na^+, K^+, and Cl^-,

employing triggers such as pH, light[32,33], voltage[34], ligands[35] and

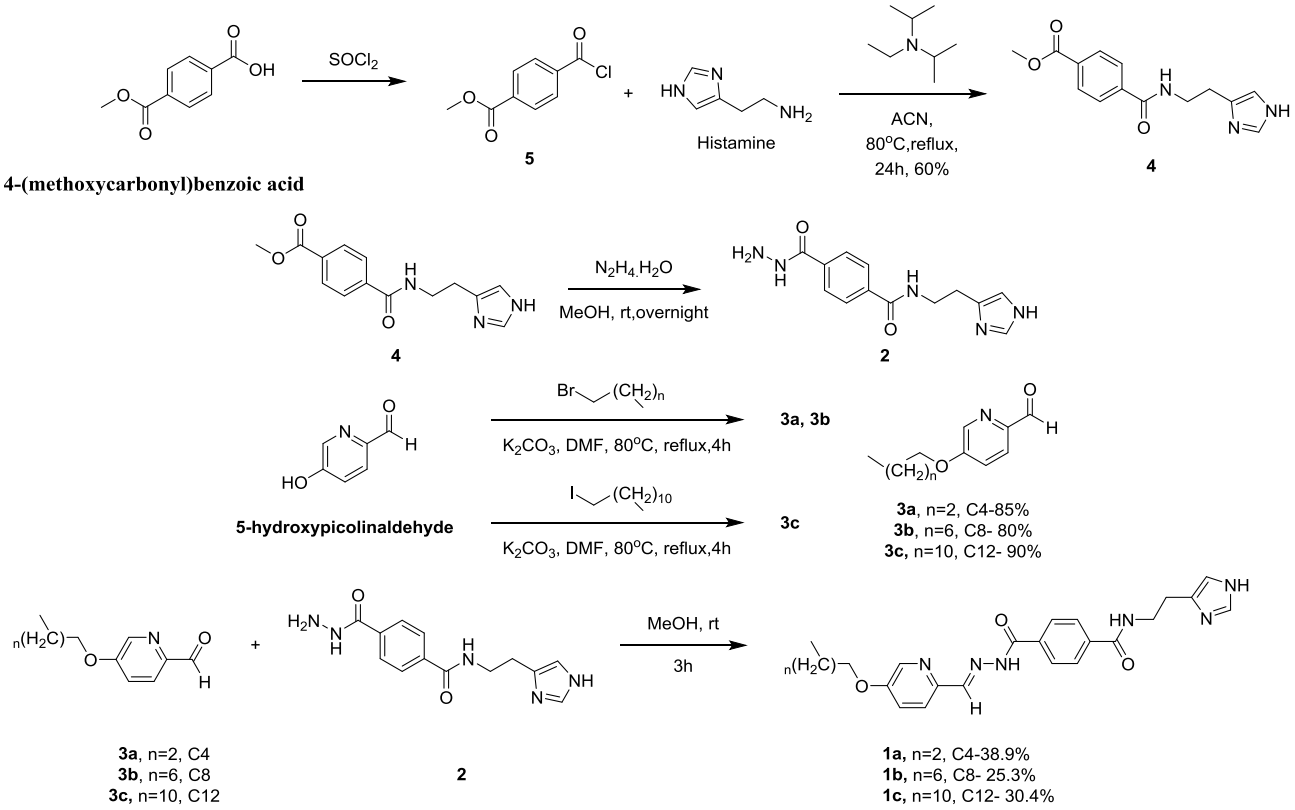

Scheme 1. Synthesis of compounds **1a-c**.

enzymes[36,37]. However, none have been specifically designed for selective proton or water transport. Among the stimuli, light-responsive ion transporters have gained significant interest due to their precise spatiotemporal control and non-invasive modulation of transport rates. Photo-switchable moieties such as acyl hydrazone[38–41], azobenzene[42,43] and stilbene[44] can enable tunable transport activity by inducing conformational changes in the structure.

Acyl hydrazones are extensively studied in medicinal chemistry as a versatile scaffold, offering structural flexibility for the development of compounds with various therapeutic applications, including antibacterial and antifungal properties[45]. They feature a dynamic imine (-C=N-) bond, capable of reversible isomerization and structural transformations under electromagnetic irradiation, endowing them with distinct photophysical properties[46]. Their facile synthesis, tunable features and ability to undergo photoinduced isomerization between *E* and *Z* configurations make them particularly suitable for designing photo-responsive ion transporters. Additionally, imidazole-based channels, which facilitate water array formation through interlayer stacking, serve as a promising functional motif for proton transport. Consequently, by designing a system where acyl hydrazones play a key role in regulating interaction patterns within the proton transport chain, it is possible to achieve precise control over transmembrane proton translocation.

Leveraging this concept, we propose an acyl hydrazone-linked imidazole-based channel forming molecule which with the help of water can form a hydrogen bonded proton transport pathway in its *E*-state while when switched to the *Z*-state can lead to the disturbance in the stacking pattern and thus modify the transport ability of the system. Herein, we report a unique self-assembled proton transport channel based on acyl hydrazone-imidazole, which exhibits distinct proton and water transport behaviour in its two isomeric states upon photoirradiation. The proposed design is first of a kind system where the proton and water transport ability of the compound are controlled via an external photoirradiation. This designed molecule shows potential as a candidate for cancer therapy owing to photo-responsive nature and may serve as a prototype for the development of future classes of stimuli-responsive water/proton transporters.

RESULTS AND DISCUSSION

Design and synthesis: The design of the synthetic proton channels incorporated imidazole, a functional group known to facilitate water wires/cluster formation, mimicking natural water channels.[47] An acyl hydrazone moiety was introduced to impart photo-switching capability to the molecule, while an adjacent pyridine ring was introduced to stabilize the *Z*-conformer after photo-switching. This stabilization occurs through intramolecular hydrogen bonding between the pyridine nitrogen and the N-H_a proton, as reported previously in the literature.[38,46,48] In addition to its photo-switching properties, the acyl hydrazone may also form hydrogen bonds with water molecules, potentially enabling the formation of proton/water channels. Further, we introduced varying alkyl chains at one end-side of the molecule as an ether connection to aid the

insertion and stabilisation of the molecule inside the membrane.

The synthetic strategy of three derivatives of the proton channel forming molecules **1a-c** involves a four-step synthetic process (Scheme 1). 4-(methoxycarbonyl) benzoic acid was transformed to its acid chloride derivative using thionyl chloride, followed by amide coupling with histamine to afford compound **4**, that was further reacted with hydrazine monohydrate in methanol to get compound **2**. Simultaneously, 5–hydroxy-picolin-aldehyde was reacted separately with 1-bromobutane, 1-bromooctane and 1-iodododecane in presence of K_2CO_3 with dimethyl formamide as a solvent under reflux condition to achieve **3a**, **3b** and **3c** respectively. **3a-c** were further separately reacted with previously synthesized molecule 2 in methanol at room temperature to give us the final channel forming molecules **1a**, **1b** and **1c** respectively. The synthesized compounds were characterised and ^1H, ^{13}C NMR and HRMS data (Figure S1-S18) are in accord with proposed structures.

Photo-switching Studies: Photo-switching studies were conducted in DMSO as a solvent in which an initial peak of absorbance at 317 nm was observed for *E* conformer for **1c** (Figure S20). Further, the system was irradiated with 310 nm LED until a photo-stationary state was achieved and a slight red shift in the absorbance peak was observed from 317 nm to 327 nm indicating a switch of isomer from *E* to *Z* (Figure 1a). The percentage of *Z* at this stage was calculated to be 80% with the help of ^1H NMR photoirradiation experiment (Figure S21). Furthermore, reverse isomerisation was done by irradiating the same sample solution with 365 nm LED to verify conversion from *Z* to *E* isomer. The spectral change during this irradiation was less pronounced than the previous irradiation, and the absorbance peak showed a minor blue shift from 327 nm to 322 nm. This shift suggests that the solution at the photo-stationary state (PSS) after 365 nm irradiation was not purely in the *E* form. The percentage of E isomer present was calculated with ^1H NMR which came out to be 46% (Figure S21). The persistence of a higher proportion of the *Z* isomer, even after 365 nm irradiation, is attributed to its enhanced stability, which is due to the strong intramolecular H-bonding between the pyridine nitrogen and the N-H_a proton (Figure 1a).

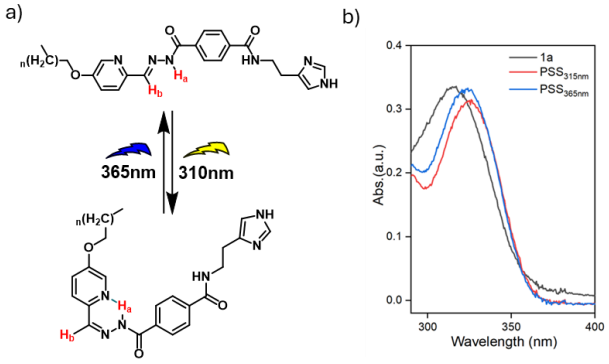

Figure 1. a) Representation of the acyl hydrazone based photo-switchable *Z* to *E* proton transporters **1a-c** and b) UV-Visible spectra of 1a in bilayer membrane vesicles and PBS solution showing spectrum at two photo-stationary state PSS stages.

To verify the photo-switching property of these compounds inside the bilayer membrane vesicles used for water/ion transport assays, compound **1a** was dissolved in 1.88 mL of phosphate buffer system with 100 µl vesicle which comprised of EYPC: Brain PS: Cholesterol 4:1:5 molar ratio mixture. The observed data was showing a similar trend as in the DMSO solvent system (Figure 1b) indicating no alteration in the photo-switching property of the compounds inside the vesicle.

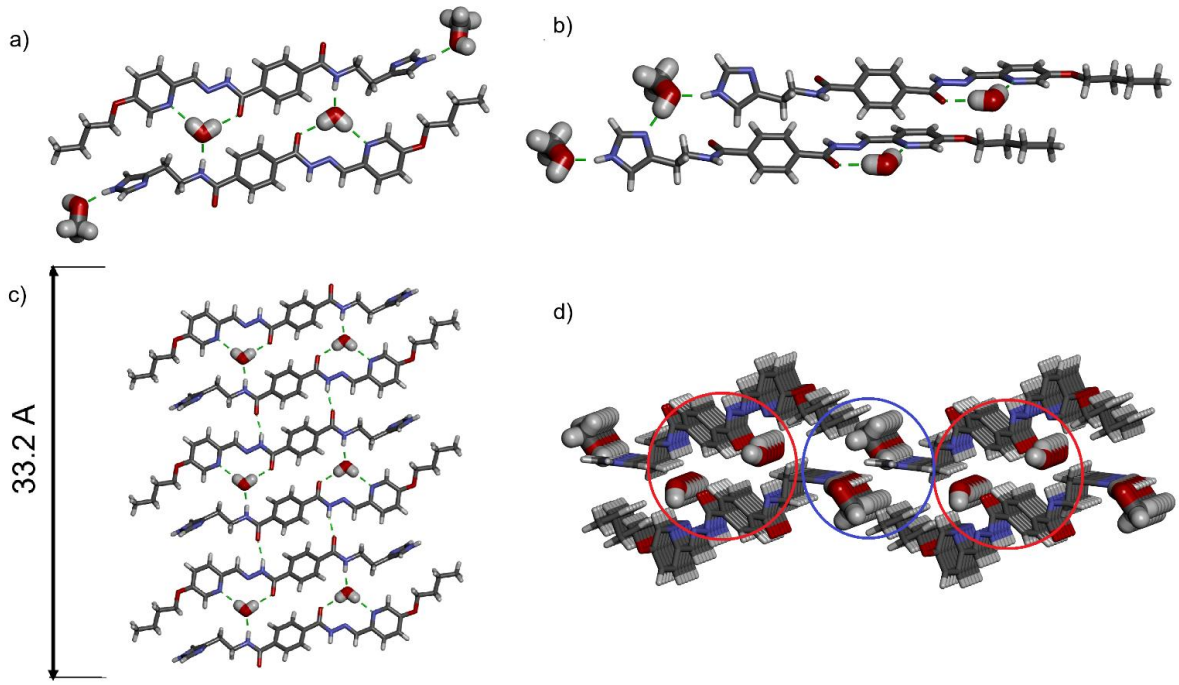

Figure 2. X-ray single crystal structures of **1a** AWCs: a) lateral and b) top view and antiparallel dimer formation with **1a** and Pyridine-hydrazone H-bonded water and imidazole H-bonded methanol molecules Structure of **U1**-channel confining 8 water molecules; c) Side and d) top view of crystal packing for **1a**-channels, confining water (red circle) and methanol (blue circle) channels showing a possible pathways for the water proton to transport.

X-ray Crystal Structure 1a: Further to understand the self-assembly behaviour that can help to understand the precise transport mechanism of proton/water through the self-assembled channels, compound **1a** was crystallised by slow evaporation (30 days) from a methanol/water solvent mixture. The X-ray structure (Table S1) revealed the formation of an antiparallel dimer of **1a**, with the terminal imidazole and alkyl groups oriented in opposite directions and stabilized as depicted in Figure 2a-c by two water molecules H-bonded to pyridine-acyl hydrazone groups of **1a**. The amide and pyridine donor acceptor H-bonds present in the molecule played a pivotal role in binding water and organizing these dimers within the same plane as these structural water molecules should be a crucial feature for the stabilization of the dimers which are further H-bonded in parallel layers. The terminal imidazole groups are hydrogen bonding methanol molecules used as solvent and stabilized via hydrophobic contacts between the methyl groups of methanol and butyl chains of **1a**. These dimers are self-assembled in a continual array via hydrazone amides resulting in the formation of a nice array of double structural water (red cercles) and methanol channels (blue cercles) that are clearly visible between the molecular planes (Figure 2d). The methanol hydrogen-bonded array forms via a combined H-bonding /hydrophobic effect. In the more dynamic self-assembly in bilayer membranes the methanol molecules can be easily replaced with water channels when embedded in the membrane providing multiple continuous water pathways, potentially facilitating proton transport across these channel structures.

Proton transport through a channel mechanism: Having confirmed the photo-switching behaviour, we performed a bilayer patch clamp study with **1a** to determine the proton channel activity of the *Z* and *E* states. Two compartments (trans and cis) containing 0.1 M HCl (pH = 1) solutions were separated by a planar lipid bilayer composed of 2-Dioleoyl-sn-glycero-3-phosphocholine (DOPC). 10 µl DMSO solution of compound 1a (5mM) was added to the grounded cis compartment and the conductance traces were recorded at an applied voltage of 80 mV across the lipid bilayer.

The conductance traces demonstrated a regular square-like signal indicating the formation of proton channels across the lipid bilayer (Figure 3a). The calculated proton conductance value for **1a** was found out to be 62 pS from the I-V plot (Figure 3b), within the range observed for synthetic ion pores.[19] This experiment illustrated the formation of proton channels by **1a** across the lipid bilayer with the conductivity of 10 times higher than M2 proton channels at pH 3[49] and is 30% of the conductivity of gramicidin A in 0.25 M HCl[26]. Additionally, the single channel proton traces revealed a transport of 2.18 $\times 10^7$ protons/channel/s (Figure S40) conducting within two order of magnitude of gramicidin at 4M HCl in symmetric conditions[50].

Furthermore, to illustrate H^+ over M^+ ion selectivity single channel current traces were recorded in unsymmetrical condition with cis chamber having 0.25 M HCl and the trans chamber containing 0.25 M MCl (M= Na^+, K^+). The I-V curve plotted for the gave us the reverse membrane potential value of -99.46 mV for Na^+ (Figure 3c) and -84.4 mV for K^+ (Figure 3d) resulting in the H^+/Na^+ selectivity of **48.1** and H^+/K^+ selectivity of **26.7** calculated from equation S6. Additionally, to demonstrate H^+ over Cl^- selectivity trans chamber was filled with 0.1 M HCl and cis chamber with 0.25 M HCl. The conductivity experiment revealed the reverse membrane potential of -46.383 mV (figure 3e) and the selectivity of H^+/Cl^- to be **81.6** derived from equation S7.

Ion Transport Studies: To study the transmembrane lipid bilayers ion transport activity, we have used egg yolk phosphatidylcholine large unilamellar vesicles entrapped with pH sensitive 8-hydroxypyrene-1,3,6-trisulfonate (HPTS) dye with 10 mM phosphate buffer system (PBS) having pH 6.4 and 100 mM NaCl salt. **1a**-**1c** with different concentration were subjected to an environment where these vesicles were suspended in 100 mM NaCl and 10 mM PBS solution. A pH difference of 1 unit (pH_{in} = 6.4 and pH_{out} = 7.4) was created across the vesicle by adding 29 µL of 0.5 M NaOH during the measurement. The emission of HPTS was monitored at 510 nm by using two excitation wavelengths 405 nm and 460 nm over a period of 360 s. After monitoring the transport activity for 280 s under the created pH gradient, Triton-X was added to the solution to disintegrate the pH gradient by lysing the vesicle and resulting in the maximum fluorescence intensity.

All the three compounds **1a**-**1c** were tested with increasing concentrations (up to 10 mM stock concentration), but the fluorescence activity did not show any significant increase in all the three cases indicating rejection of NaCl salt (Figure S23). Then the ion transport activity of the compounds was further evaluated using various external cations (Li^+, K^+, Rb^+, Cs^+) to assess their ability to reject other cationic salts at a similar concentration. A 2 mM stock solution of compounds **1a**–**1c** was exposed to NaCl-entrapped vesicles suspended in solutions containing different salts, including NaCl, KCl, LiCl, RbCl, and CsCl. Fluorescence monitoring revealed a negligible increase in fluorescence activity, indicating complete salt rejection for all tested cations (Figure 4a, Figure S24). This finding prompted further investigation of the ion transport capability of these compounds in a similar setup, following a conformational switch to the **1a-*Z***-isomer upon irradiation with 310 nm LED light. The irradiation was performed for 2 minutes after which the compound was added to the vesicles and PBS solution.

Post-irradiation, the fluorescence intensity was measured under a pH gradient over the same time as in the initial conditions. Interestingly, compound **1b-*Z*** demonstrated a slight increase in fluorescence intensity, reaching up to 0.4 for certain cations indicating and optimal channel self-assembly / dynamic aggregation behaviours provided by

the octyl chains, resulting in an optimal channel-ion transport activity after photo-switching (Figure S25a), while compounds **1a-*Z*** (Figure 4b) and **1c-*Z*** remained completely inactive toward all tested cations (Figure S25b). After confirming the cation-independent behaviour of these systems, we proceeded to investigate the involvement of anions in the ion transport process by using different external salts, including NaCl, NaBr, NaI, NaOMe, and $NaNO_3$. The results demonstrated no activity for any of the compounds with.

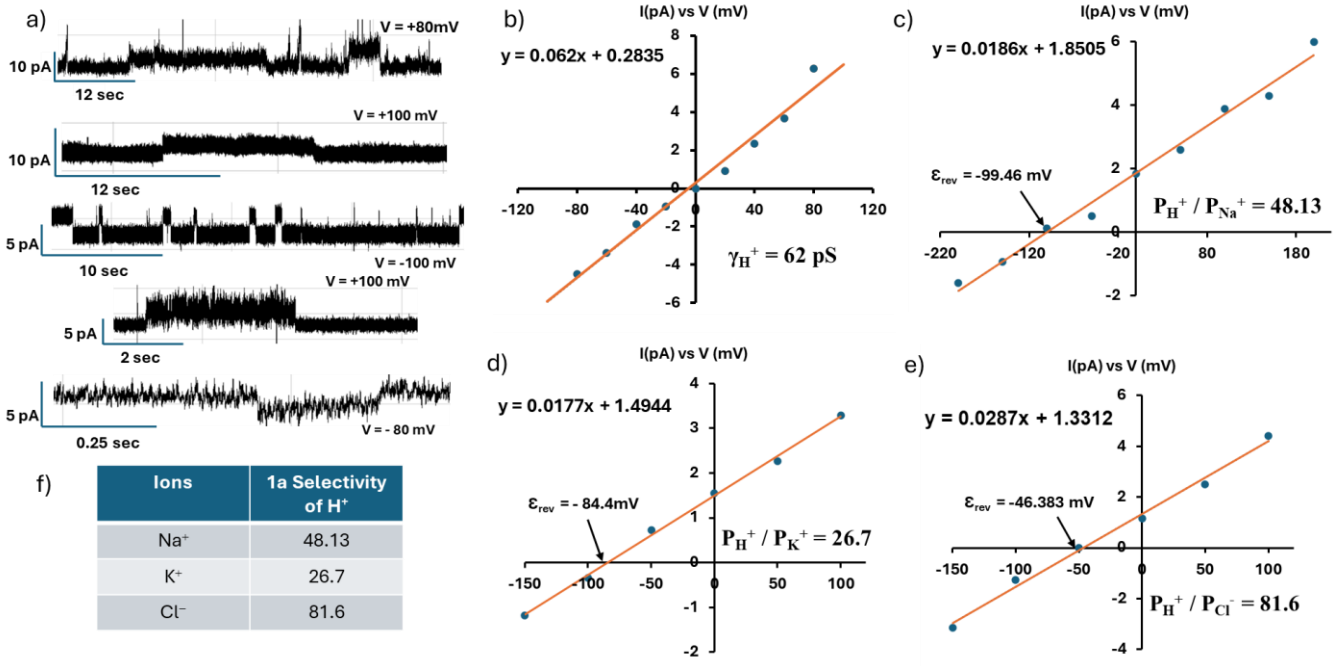

f)

Ions	1a Selectivity of H^+
Na^+	48.13
K^+	26.7
Cl^-	81.6

Figure 3: a). The single channel current traces observed (from the top) i) under symmetric condition at +80 mV with 0.1 M HCl in both cis and trans chamber ii) For unsymmetric conditions at +100 mV with 0.25 M HCl in cis chamber and 0.25 M NaCl in trans iii) The next two traces observed at -100 mV and +100 mV sequentially for 0.25 M HCl in cis and 0.25 M KCl in trans iv) unsymmetric condition at -80 mV with 0.25 M HCl in cis chamber and 0.1 M HCl in trans. b) The conductivity experiment for symmetric condition for **1a**. Conductivity experiment for unsymmetric conditions to determine the selectivity of c) H^+ over Na^+, d) H^+ over K^+ and e) H^+ over Cl^- , f) The table summarising the selectivity of **1a** for H^+ over other ions.

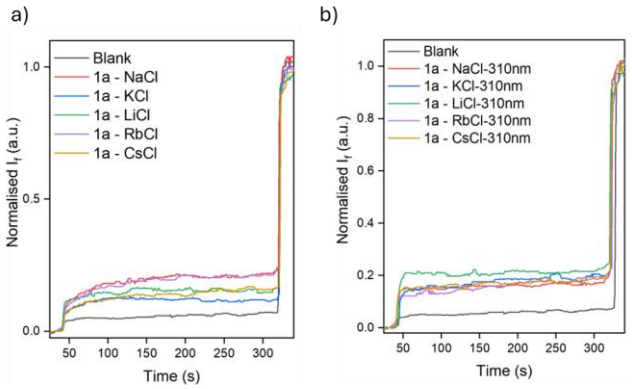

Figure 4: a) Ion transport activity of a) **1a-*E*** (2mM) and of b) **1a-*Z*** (2mM) after irradiation of 310 nm light in EYPC-LUVs ⊃ HPTS and internal NaCl and in presence of different external cationic salts.

these anions, indicating the rejection of anions as well (Figure S26). Additionally, the anion transport capability of the photo-switched **1a-*Z*-c-*Z*** -conformers was evaluated using NaCl, NaI, NaBr, and NaOMe.

None of the compounds exhibited a significant increase in salt transport activity, further confirming the rejection of the tested salts in their photo-switched forms (Figure S27).

Further, K^+ and H^+- assisted valinomycin and FCCP assays were conducted to evaluate the transport activity of the compounds **1a**-**1c** under electrogenic membrane-polarization experiments. FCCP (Carbonyl cyanide-p-trifluoromethoxyphenylhydrazone) a synthetic protonophore known for transporting proton across the membrane was used in combination with different external salts, which would result in an H^+/M^+ antiport if M^+ transport was carried out by **1a**-**1c** in the opposite direction to proton transport carried out via FCCP.

The results indicated that no M^+ transport was observed for the E conformer of **1a-*E*-1c-*E*** (Figure S28). Similarly, the *Z* conformers of **1a-*Z*** and **1c-*Z*** displayed no evidence of M^+ transport after photo-switching, showing results consistent with the *E* conformers. However as previously observed, for **1b-*Z***, a slight increase in transport activity was observed post-photo-switching, suggesting an optimal contribution to the H^+/M^+ antiport mechanism (Figure S29).

Additionally, the proton transport assay was carried out to elucidate the proton transport ability of **1a**-**1c** in, the presence of Valinomycin. Valinomycin (12.5 μM) was added to the vesicle solution as a K+ carrier in addition to these compounds and we observed a H^+/K^+ antiport with an increase in the transport activity indicating proton transport for all compounds **1a**-**1c** (Figure 5a). These led us to calculate the half maximal effective concentration (EC50) of these compounds for proton transport. The value at 310 sec of the fluorescence reading was used for the hill equation plot (Figure 5b) and the EC50 values found were 15.24 ± 1.74 μM, 3.72 ± 0.29 μM and 13.91 ± 1.30 μM for 1a, 1b and 1c respectively (Figure 5c). These values indicate the proton transport among 1a-1c follows the sequence **1b** > **1c** > **1a**. Hill coefficient values calculated for **1a**, **1b** and **1c** were 1.27, 2.82 and 1.83 respectively. All the n values were greater than 1 implying a positive cooperativity in the self- assembly process.[51]

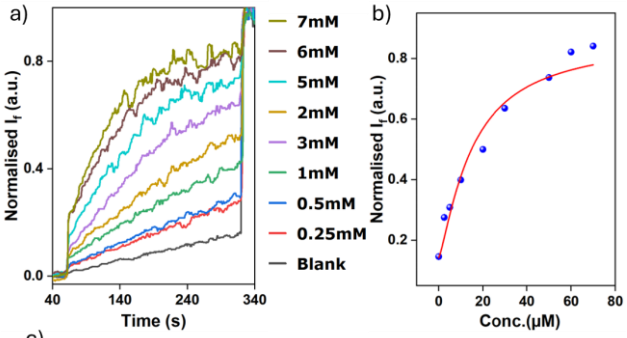

c)

Molecule	EC_{50}	Hill Coefficient (n)	Log P
1a	15.24 ± 1.74 μM	1.27	2.61
1b	3.72 ± 0.29 μM	2.81	3.98
1c	13.91 ± 1.30 μM	1.83	5.47

Figure 5: a) Proton transport activity of **1a** with increasing concentration (0–7mM of stock solution) in presence of Valinomycin (25 uM), b) the corresponding hill plot at t = 310 sec and c) the EC50 and the hill coefficient (n) values calculated from the hill equation for each compound **1a-1c** and their corresponding log P values as obtained from (http://www.swissadme.ch/index.php).

Light response on proton transport rate: The promising results from the valinomycin assay prompted us to investigate the effect of photo-switching on transmembrane proton transport. For this, sequential irradiation with 310 nm and 365 nm LEDs was performed on bilayer vesicle solution incorporating **1a**-**1c** and the proton transport rate was monitored after each irradiation. A concentration exhibiting a proton transport activity around 0.5 for each compound was selected for this assay. For each compound **1a**-**1c**, the sample was first irradiated with 310 nm to induce the formation of *Z* conformer, and at the photostationary state (PSS), and notably a significant increase in proton transport rate was observed. Subsequently, the *Z* conformer was irradiated with 365 nm, which resulted in a decrease in proton transport rate (Figure 6a). The fluorescence values at 190 s were plotted for each compound after irradiation with 310 nm and subsequent 365 nm irradiation for comparison (Figure 6b). These findings indicate that proton transport is more efficient in the *Z* conformer compared to the *E* conformer. For more detailed information about this photo-switching effect, water transport studies were carried out.

Light response on water transport rate: To determine the water transport ability of the compounds **1a**-**1c** they were reconstituted in a phosphatidylcholine (PC)/ phosphatidylserine (PS)/ cholesterol (Chl) mixture with a molar ratio of 4:1:5 obtaining vesicles with a 100 nm diameter **1a**, **1b** and **1c** were added from the DMSO solution with different concentrations to the vesicle suspensions in 200 mM D(+)- sucrose osmolyte and 10 mM PBS solution (pH = 6.4). The solution was incubated for 30 min after which these vesicles were subjected to hypertonic condition of 400 mM D(+)- sucrose solution, creating a water gradient to force the water to get out of the vesicles. The resulting rate of shrinkage of the vesicles was monitored by the increase in the light scattering signal. A concentration dependent study with three different mCLR of 0.01136 (0.5 mM stock), 0.02326 (1 mM stock) and 0.04651 (2 mM stock) revealed negligible increase in the water transport rates (Figure S34-S36). The process was further repeated after the irradiation of the compounds **1a**-**1c** (1mM stock concentration) vesicle solutions with 310 nm LED and subsequently after 365 nm LED irradiation, giving us the effect of photo-switching on water transport rate for the molecules (Figure 6c). The net permeability values were calculated for each compound **1a**-**1c** and after each irradiation which gave us the rate of transport of water through the vesicle membrane. For a molar compound to lipid ratio of 0.023 (1mM stock solution) the initial net permeability values were found to be 2.56 μm/s, 3.19 μm/s and 3.71 μm/s for **1a**, **1b** and **1c** respectively. The low net permeability values for the **1a**-***E***-**1c**-***E*** conformers can be explained as the water molecules are strongly embedded in within interlayers within red (red) acylhydrazone- and (blue) imidazole channels (see Figure 2d) as observed in the crystal structure resulting in the formation of no continuous water arrays to facilitate the water transport. Interestingly, the net permeability values increase significantly after irradiation with 310 nm light for 1.5 min indicating that the **1a**-***Z***-**1c**-***Z*** conformer results in increased rate of water transport as compared to the **1a**-***E***-**1c**-***E*** conformer. The net permeability values were 13.64 μm/s, 7.19 μm/s and 10.57 μm/s for **1a**-***Z***, **1b**-***Z*** and **1c**-***Z*** respectively after irradiation with 310 nm LED. To check the effect of reverse isomerisation on the water transport rate the *Z* conformer solution was further irradiated with 365 nm LED and notably the net permeability values decreased to 7.2 μm/s, 6.21 μm/s, 4.18 μm/s respectively for **1a**-***E***, **1b**-***E*** and **1c**-***E*** (Figure 6d). We further calculated the single channel permeability (P_s) of these channels based on the net permeability values obtained from the experiment. For mCLR of 0.023 and assuming 6 molecules are required to span the membrane length of 35 Å (Figure 2c), the P_s value ranges in between 0.65×10^7 - 0.94×10^7 water molecules/s/channel. The P_s values increased noticeably to 1.8×10^7 - 3.5×10^7 water molecules/s/channel after irradiation with 310 nm. However, a further decrease in the P_s value was observed to 1.06×10^7 - 1.8×10^7 water molecules/s/channel after irradiating with 365 nm LED (Table S2). We note that for all transport experiments successive irradiations from *E*-conformers to *Z*-conformers and back to the *E*-conformers are not leading to pure *E*-conformers, suggesting the slow re-*Z*→*E* isomerization led to a mixture of *E*-Z conformers, as previously observed with other carriers.[44] These findings indicate that as for the proton transport rates, the water transport rates are significantly higher in the *Z*-conformers compared to the *E*-conformers. This difference in permeability can be attributed to the structural flexibility of the bended *Z*-conformer.

Specifically, in the *Z*-conformer the structural water molecules are expulsed, the absence of an additional amide bond for interlayer bonding results in a less rigid bended molecular architecture. This reduced rigidity allows the *Z*-conformer to adopt a more dynamic configuration, facilitating easier water and proton dynamics and diffusion through the imidazole channel. In contrast, the *E*-conformer, due to the accessibility of the amide bond for interlayer stacking, it exhibits increased rigidity and a

more constrained layered structure. This rigidity likely hinders the movement of water molecules, resulting in a lower permeability.

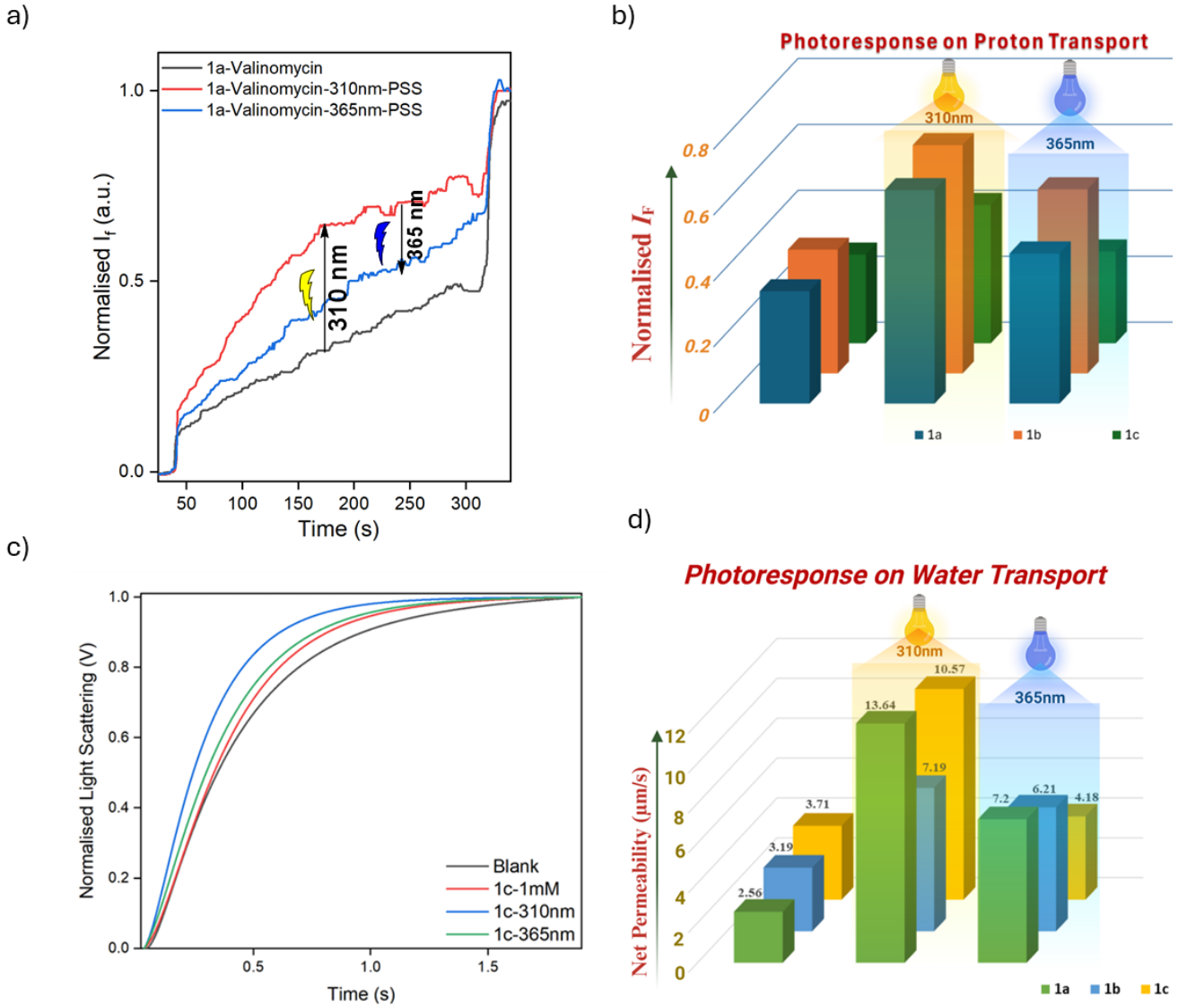

Figure 6: a) The fluorescence assay for compound **1a** in presence of valinomycin and the change in graph after irradiation with 310 nm and 365 nm LEDs; b) 3D graphs showing the change in the ion transport activity for compounds **1a**-**1c** at 190 s during the assay after irradiation with 310 nm and 365 nm LEDs. c) Stopped flow light scattering experimental data for **1c** at 1mM concentration showing the changes in the normalised curves after irradiating with 310 nm and 365nm light and d) 3D graphs indicating the changes in net permeability for compounds 1a, 1b and 1c after irradiation with 310 nm and 365 nm LEDs.

These results can also be correlated to the proton transport results where the Z conformer is more responsible for proton transport indicating that the proton in this case is travelling with water as opposed to the *E* state where it was hopping through the molecule and water H-bonded network in the imidazole channels. The proton diffusion along H-bonded water chains needs certain dynamic behaviours of the water-imidazole chains to reorient and facilitate the proton translocation.[52] Thus, proving that photo-switching in between the *Z*- and *E*-conformers plays a crucial role in modulating water and proton transport efficiency, with the *Z*-conformer providing a more favourable pathway for water diffusion through the membrane. Furthermore, a comparative analysis of proton-to-water transport selectivity was conducted for compound **1a** to quantitatively assess its transport behavior following successive photoirradiation steps. This selectivity was derived by combining patch-clamp measurements with fluorescence-based photoswitching data obtained from Figure **6a**. The results indicated an initial proton-over-water selectivity of **3.35** prior to irradiation (Table S3), suggesting that protons were transported approximately three times more efficiently than water through the channels. Upon irradiation at **315 nm**, the selectivity remained similar at **3.14** but further decreased to **2.00** after exposure to **365 nm** light. The data consistently indicated that proton transport was favored over water under all irradiation conditions. For further clarification on this and to study the mechanis-

tic pathway of proton and water transport we carried out exploratory molecular dynamics (MD) simulation studies.

Molecular Dynamics Simulations: Considering that transmembrane transport is an inherently dynamic process, and the X-Ray structure is only a snapshot of dynamic self-assembly behaviours of channels in the bilayer membrane, we deemed it essential to perform Molecular Dynamics (MD) simulations in order to gain a more realistic atomic-level understanding of water/proton translocation events. We extracted a small patch (mCLR of 0.151) from the resolved molecular structure of **1a-*E*** and inserted into the POPC membrane. When methanol was removed from the single crystal X-ray molecular structure, intriguingly, these cavities of **1a-*E*** channels were spontaneously filled with water to create potential water/ proton transport pathways (Figure 7a). A close inspection of the water distribution within the initial channel configuration (i.e., t = 0 ns) revealed a water-imidazole array with complementary H bonds. Here, each water molecule serves as a bridge between two imidazole head groups of parallelly stacked **1a** units (Figure 7a). Importantly, imidazole-intercalated water molecules are not crucial for the stability of the self-assembly aggregate, in contrast to the water molecules presented within acylhydrazone channels. Specifically, MD runs without any

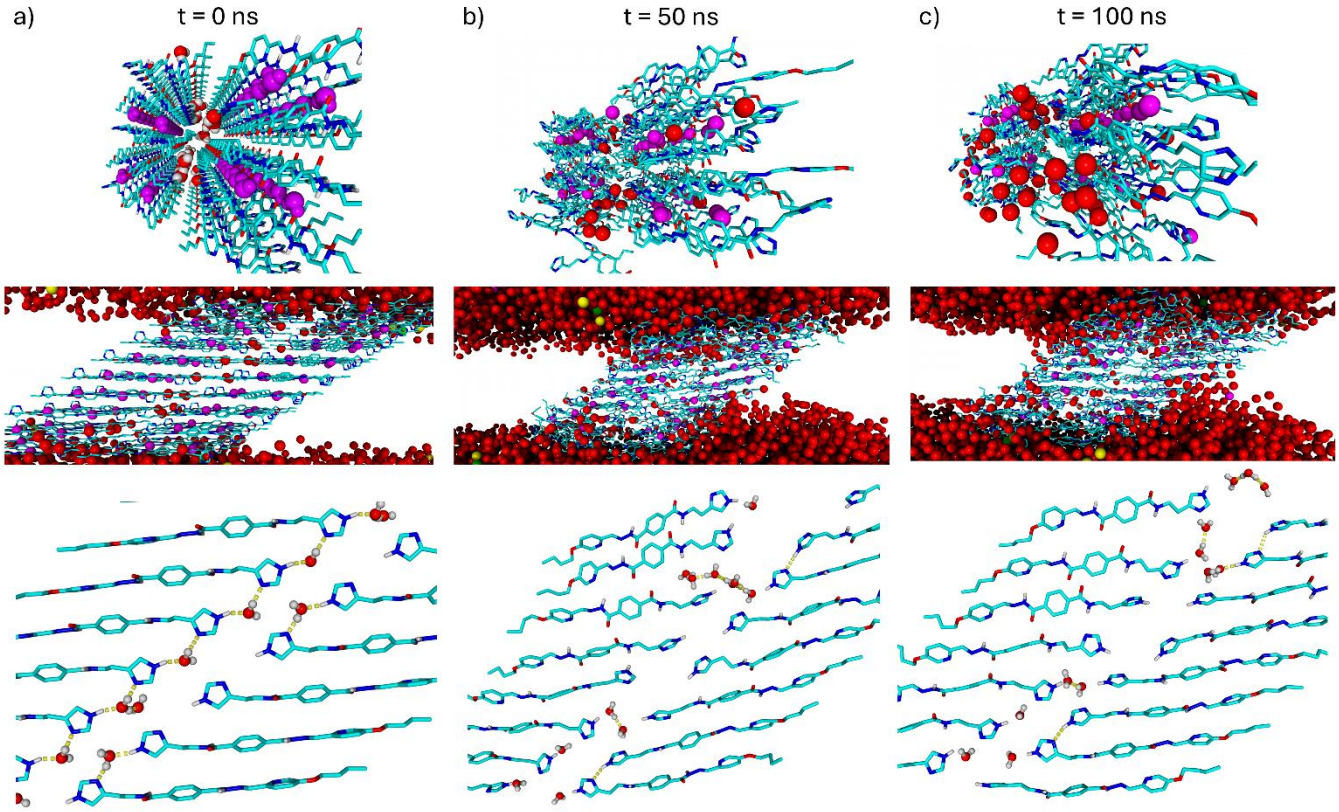

Figure 7. MD simulation snapshots of **1a-*E*** within a POPC membrane at a) t = 0 ns, b) 50 ns and c) 100 ns illustrating the stability of the self-assembled channels within bilayer membrane environment over time and highlighting the imidazole water/proton translocation pathway. Water molecules within the self-assembled imidazole channels are depicted in magenta to distinguish them from structural water molecules strongly bonded to arylhydrazone moieties and bulk water molecules. Hydrogen atoms have been omitted for clarity.

constraints demonstrate that beyond the temporal stability of the self-assembled aggregate, imidazole head groups can stabilize each other (Figure 7b,c). We observe the formation of temporary stabilized water wires that sustain a water/hydronium ion hopping translocation mechanism. The observed channel pathway is more favourable for water/proton over other ions due to the presence of alternating Hydrogen bond donor (N-H groups) and hydrogen bond acceptor groups (Imidazole-N) and the less conducive environment for anion and cation binding explains ion rejection by the system. Analysis of the channel's inner imidazole binding motifs indicates a strong preference for coordinating water molecules over other ions, in agreement with previous observations from I-quartet channels reported by our group.[30,47] In this arrangement, the alternating N–H and N functionalities establish a sequential hydrogen bond donor–acceptor environment (Figure 7), which is optimally suited to stabilize water clusters beside coordinating the cations and anions. In contrast, efficient cation binding would necessitate the presence of at least two closely positioned hydrogen bond acceptors to provide an energetically favourable electrostatic interaction, a feature absent in this channel. A similar limitation applies to anion binding, where two or more proximal hydrogen bond donors are typically required to accommodate and transport larger anions such as chloride, which is likewise not supported by the channel's architecture. Taken together, these structural features strongly suggest that the channel is inherently selective for water and proton transport, while effectively excluding both cations and anions.

Notably, the structural water molecules intercalated within the acylhydrazone layers are and remain tightly bound during overall simulations, being crucial for self-assembly but not undergoing translocation. Notably, due to the stabilisation of the antiparallel strongly packed configuration by the *E* isomer (see Figure 2c), a dynamic configuration where imidazole groups cooperate together to form a dynamic I -quartet is partially hindered. Although no direct simulations of the Z configuration were performed, as no structural data is available, it can be deduced that when switching the assembly observed in the simulations of the E configuration to the *Z* configuration, water access to the acylhydrazone would be restricted, which destroys the highly packed antiparallel stacking. As a result, there is a higher likelihood of formation of more dynamic imidazole-quartets that support faster water and proton transport across the lipid bilayer. Consequently, these findings effectively (yet indirectly) reaffirm the experimentally observed lower water and proton translocation rates of the *E*-state as compared to the *Z*-state.

Complementarily, membrane insertion efficiency experiments were conducted to evaluate the incorporation behaviour of the molecule in its different conformational states. The same vesicles used in the water transport assays were employed, and insertion efficiency was quantified based on concentration curves derived from UV–Vis spectroscopy for both isomers (Figures S45–S50). The results revealed that membrane insertion efficiency increased significantly upon switching from the E to the Z conformer (Table S4), suggesting that the observed differences in water and proton transport rates are influenced not only by the intrinsic binding characteristics of the isomers but also by their differential membrane incorporation.

CONCLUSION

In this study, we demonstrated light-responsive proton and water channels whose transport rates can be externally controlled using light radiation. The synthesized channels exhibited efficient photoswitching, as confirmed by UV-Vis and ^{1}H NMR studies. Furthermore, proton channel formation was validated using patch clamp assays exhibiting a proton transport rate of 2.18 ×10^7 H^+ per second per channel. Additionally, the ion selectivity through patch clamp assay for **1a** revealed a high selectivity of H^+ over Na^+, K^+, Cl^- ions with a value of 48.13, 26.7 and 81.6 respectively. The crystal structure of **1a-*E*** revealed a novel proton transport pathway mediated by water molecules in two different amide and imidazole channels. The HPTS assay with various external cations and anions indicated salt rejection for both *E* and *Z* conformers across all compounds, except for minimal activity observed with **1b**. The valinomycin-assisted assay revealed efficient proton transport, with **1b** showing the lowest half-maximal concentration (3.73 ± 0.29 μM). Photo-responsive tests confirmed increased proton transport upon switching to the *Z* conformer and a subsequent decrease upon reverting to the *E* conformer. The stopped flow assay revealed a similar trend in the transport rate of water, as for proton transport where *Z* conformer was responsible for increased rate of water transport up 3.5×10^7 water molecules/s/channel after irradiation with 310 nm, one order the magnitude less than natural Aquaporins. Molecular Dynamics simulations of **1a-*E*** revealed that the primary transport pathway for the transport of water and proton is through imidazole and the embedded water remains stationary resulting in an increased rigidity of the system. Through this we can interpret that the photo switched *Z* conformer's increased proton and water transport behaviour is due to the intrinsic change in the interaction pattern with water molecule rendering the system more dynamic and responsive towards water/ proton transport. Along with the intrinsic interaction changes, the membrane incorporation ability of the molecules significantly increases after switching from *E* to *Z* conformer which again adds to the increased transport rate for the Z isomer.

Proton selectivity and gating/pumping are the key functions of Influenza A M2,[53] or to the light-driven microbial rhodopsins[54] proton channels. Selective artificial proton channels are less described in literature. Biomimetic I-quartets reported by our group a decade ago remained long time as unique selective proton channels *via* artificial water channels,[30] while nowadays new discoveries in this field are being made. Designing exclusive proton flux through lipid bilayers remains a challenging task.[26,55,-56] The findings described in this paper add a new advancement to this field establish an impressive light-responsive system capable of regulating proton and water transport through biomimetic channels with potential implications for light-controlled artificial water/proton channel systems. This system also shows promise in cancer treatment owing to their photoresponsive nature and can be essentially helpful in designing future class of stimuli responsive and selective proton /water channels a field which is largely unexplored.

▪ ASSOCIATED CONTENT

Supporting Information.

Materials and Methods, synthetic procedures for 1a-1c, NMR and HRMS data, SCXRD data, patch clamp, stopped flow assay, fluorescence spectrums, UV-Visible spectrum is available in the supporting information.

The Supporting Information is available free of charge on the ACS Publications website.

▪ AUTHOR INFORMATION

Corresponding Author

***Mihail Barboiu –** *Institut Europeen des Membranes* (IEM), *Adaptive Supramolecular Nanosystems Group* (NSA), *University of Montpellier*, 34095 *Montpellier, France*; Email : mihail-dumitru.barboiu@umontpellier.fr

Authors

Paras Wanjari – *Institut Europeen des Membranes* (IEM), *Adaptive Supramolecular Nanosystems Group* (NSA), *University of Montpellier*, 34095 *Montpellier, France*

Ionut Stroia – *Institut Europeen des Membranes* (IEM), *Adaptive Supramolecular Nanosystems Group* (NSA), *University of Montpellier*, 34095 *Montpellier, France*

Arie van der Lee – *Institut Europeen des Membranes* (IEM), *Adaptive Supramolecular Nanosystems Group* (NSA), *University of Montpellier*, 34095 *Montpellier, France*

Marc Baaden – Université Paris Cité, CNRS, Laboratoire de Biochimie Théorique, 13 rue Pierre et Marie Curie, 75005, Paris, France

- **Notes**

  The authors declare no competing financial interest.

ACKNOWLEDGEMENT

This project has received funding from the European Union's Horizon 2020 research and innovation program under the Marie Skłodowska-Curie grant agreement No 860592" and the Agence Nationale de la Recherche (ANR) grant ANR-23-CE06-0030, AQUAFOLDAMERS.

REFERENCES

(1) Williams, K. A. Three-Dimensional Structure of the Ion-Coupled Transport Protein NhaA. *Nature* **2000**, *403* (6765), 112–115.

(2) Zhang, Q.; Jian, L.; Yao, D.; Rao, B.; Xia, Y.; Hu, K.; Li, S.; Shen, Y.; Cao, M.; Qin, A.; Zhao, J.; Cao, Y. The Structural Basis of the pH-Homeostasis Mediated by the Cl−/HCO3− Exchanger, AE2. *Nat. Commun.* **2023**, *14* (1), 1812.

(3) Skou, J. Chr. The Influence of Some Cations on an Adenosine Triphosphatase from Peripheral Nerves. *Biochim. Biophys. Acta* **1957**, *23*, 394–401.

(4) Rieger, B.; Junge, W.; Busch, K. B. Lateral pH Gradient between OXPHOS Complex IV and F0F1 ATP-Synthase in Folded Mitochondrial Membranes. *Nat. Commun.* **2014**, *5* (1), 3103.

(5) Surmeier, D. J.; Guzman, J. N.; Sanchez-Padilla, J.; Schumacker, P. T. The Role of Calcium and Mitochondrial Oxidant Stress in the Loss of Substantia Nigra Pars Compacta Dopaminergic Neurons in Parkinson's Disease. *Neuroscience* **2011**, *198*, 221–231.

(6) Ashcroft, F. M.; Puljung, M. C.; Vedovato, N. Neonatal Diabetes and the KATP Channel: From Mutation to Therapy. *Trends Endocrinol. Metab.* **2017**, *28* (5), 377–387.

(7) Wemmie, J. A.; Taugher, R. J.; Kreple, C. J. Acid-Sensing Ion Channels in Pain and Disease. *Nat. Rev. Neurosci.* **2013**, *14* (7), 461–471.

(8) Elborn, J. S. Cystic Fibrosis. *The Lancet* **2016**, *388* (10059), 2519–2531.

(9) Marunaka, Y. The Role of Ion-Transporting Proteins in Human Disease. *Int. J. Mol. Sci.* **2024**, *25* (3), 1726.

(10) Yang, J.; Yu, G.; Sessler, J. L.; Shin, I.; Gale, P. A.; Huang, F. Artificial Transmembrane Ion Transporters as Potential Therapeutics. *Chem* **2021**, *7* (12), 3256–3291.

(11) Salunke, S. B.; Save, S. N.; Roy, N. J.; Naorem, R.; Sharma, S.; Talukdar, P. Bisindole-Based Small Molecules as Transmembrane Anion Transporters and Potential Anticancer Agents. *Org. Biomol. Chem.* **2024**, *22* (24), 4987–4992.

(12) Gilchrist, A. M.; McNaughton, D. A.; Fares, M.; Wu, X.; Hawkins, B. A.; Butler, S. J.; Hibbs, D. E.; Gale, P. A. Tetralactam-Based Anion Transporters. *Chem* **2025**, *11* (1).

(13) Rather, I. A.; Ahmad, M.; Talukdar, P.; Ali, R. Probing and Evaluating Transmembrane Chloride Ion Transport in Double Walled Trifluorophenyl/Phthalimide Extended Calix [4] Pyrrole-Based Supramolecular Receptors. *J. Mater. Chem. B* **2024**,*12*, 5950-5956.

(14) Chattopadhayay, S.; Ghosh, A.; Kumar Mukhopadhyay, T.; Sharma, R.; Datta, A.; Talukdar, P. Supramolecular Barrel-Rosette Ion Channel Based on 3,5-Diaminobenzoic Acid for Cation-Anion Symport. *Angew. Chem.* **2023**, *135* (46), e202313712.

(15) Andrei, I. M.; Chaix, A.; Benkhaled, B. T.; Dupuis, R.; Gomri, C.; Petit, E.; Polentarutti, M.; van der Lee, A.; Semsarilar, M.; Barboiu, M. Selective Water Pore Recognition and Transport through Self-Assembled Alkyl-Ureido-Trianglamine Artificial Water Channels. *J. Am. Chem. Soc.* **2023**, *145* (39), 21213–21221.

(16) Mondal, A.; Mondal, D.; Sarkar, S.; Shivpuje, U.; Mondal, J.; Talukdar, P. Self-Assembled Hydrazide-Based Nanochannels: Efficient Water Translocation and Salt Rejection. *Angew. Chem.* **2025**, *137* (3), e202415510.

(17) Mondal, D.; Dandekar, B. R.; Ahmad, M.; Mondal, A.; Mondal, J.; Talukdar, P. Selective and Rapid Water Transportation across a Self-Assembled Peptide-Diol Channel via the Formation of a Dual Water Array. *Chem. Sci.* **2022**, *13* (33), 9614–9623.

(18) Shen, J.; Ye, R.; Romanies, A.; Roy, A.; Chen, F.; Ren, C.; Liu, Z.; Zeng, H. Aquafoldmer-Based Aquaporin-like Synthetic Water Channel. *J. Am. Chem. Soc.* **2020**, *142* (22), 10050–10058.

(19) Su, D.; Ulrich, S.; Barboiu, M. Bis-Alkylureido Imidazole Artificial Water Channels. *Angew. Chem.* **2023**, *135* (35), e202306265.

(20) Pérez-Pérez, M.; Fuertes, A.; Montenegro, J. Synthetic Peptide Scaffolds as Ion Channels and Molecular Carriers. *Curr. Opin. Chem. Biol.* **2025**, *84*, 102563.

(21) Li, X.; Zhang, H.; Hou, J.; Ou, R.; Zhu, Y.; Zhao, C.; Qian, T.; Easton, C. D.; Selomulya, C.; Hill, M. R.; Wang, H. Sulfonated Sub-1-Nm Metal–Organic Framework Channels with Ultrahigh Proton Selectivity. *J. Am. Chem. Soc.* **2020**, *142* (21), 9827–9833.

(22) Andrei, I. M.; Chen, W.; Baaden, M.; Vincent, S. P.; Barboiu, M. Proton- versus Cation-Selective Transport of Saccharide Rim-Appended Pillar[5]Arene Artificial Water Channels. *J. Am. Chem. Soc.* **2023**, *145* (40), 21904–21914.

(23) Tawa, G. J.; Topol, I. A.; Burt, S. K.; Caldwell, R. A.; Rashin, A. A. Calculation of the Aqueous Solvation Free Energy of the Proton. *J. Chem. Phys.* **1998**, *109* (12), 4852–4863..

(24) Mandala, V. S.; Liao, S.-Y.; Kwon, B.; Hong, M. Structural Basis for Asymmetric Conductance of the Influenza M2 Proton Channel Investigated by Solid-State NMR Spectroscopy. *J. Mol. Biol.* **2017**, *429* (14), 2192–2210.

(25) Si, W.; Chen, L.; Hu, X.-B.; Tang, G.; Chen, Z.; Hou, J.-L.; Li, Z.-T. Selective Artificial Transmembrane Channels for Protons by Formation of Water Wires. *Angew. Chem. Int. Ed.* **2011**, *50* (52), 12564–12568.

(26) Shen, J.; Ye, R.; Liu, Z.; Zeng, H. Hybrid Pyridine-Pyridone Foldamer Channels as M2-Like Artificial Proton Channels. *Angew. Chem. Int. Ed Engl.* **2022**, *61* (28), e202200259.

(27) Agmon, N. The Grotthuss Mechanism. *Chem. Phys. Lett.* **1995**, *244* (5), 456–462.

(28) Yan, T.; Liu, S.; Xu, J.; Sun, H.; Yu, S.; Liu, J. Unimolecular Helix-Based Transmembrane Nanochannel with a Smallest Luminal Cavity of 1 Å Expressing High Proton Selectivity and Transport Activity. *Nano Lett.* **2021**, *21* (24), 10462–10468.

(29) Gu, W.; Zhou, B.; Geyer, T.; Hutter, M.; Fang, H.; Helms, V. Design of a Gated Molecular Proton Channel. *Angew. Chem. Int. Ed.* **2011**, *50* (3), 768–771.

(30) Le Duc, Y.; Michau, M.; Gilles, A.; Gence, V.; Legrand, Y.-M.; van der Lee, A.; Tingry, S.; Barboiu, M. Imidazole-Quartet Water and Proton Dipolar Channels. *Angew. Chem.* **2011**, *123* (48), 11568–11574.

(31) Jiang, T., Hall, A., Eres, M. *et al.* Single-chain heteropolymers transport protons selectively and rapidly | Nature.**2020**, *577,* 216-220.

(32) Ahmad, M.; Gartland, S. A.; Langton, M. J. Photo- and Redox-Regulated Transmembrane Ion Transporters. *Angew. Chem. Int. Ed.* **2023**, *62* (44), e202308842.

(33) Chattopadhayay, S.; Banzal, K. V.; Talukdar, P. Photo-Activation of Tolane-Based Synthetic Ion Channel for Transmembrane Chloride Transport. *Angew. Chem. Int. Ed.* **2025**, *64* (2), e202414354.

(34) Kobuke, Y.; Ueda, K.; Sokabe, M. Totally Synthetic Voltage Dependent Ion Channel. *Chem. Lett.* **1995**, *24* (6), 435–436.

(35) Talukdar, P.; Bollot, G.; Mareda, J.; Sakai, N.; Matile, S. Ligand-Gated Synthetic Ion Channels. *Chem. – Eur. J.* **2005**, *11* (22), 6525–6532.

(36) Choi, Y. R.; Lee, B.; Park, J.; Namkung, W.; Jeong, K.-S. Enzyme-Responsive Procarriers Capable of Transporting Chloride Ions across Lipid and Cellular Membranes. *J. Am. Chem. Soc.* **2016**, *138* (47), 15319–15322.

(37) Malla, J. A.; Umesh, R. M.; Yousf, S.; Mane, S.; Sharma, S.; Lahiri, M.; Talukdar, P. A Glutathione Activatable Ion Channel Induces Apoptosis in Cancer Cells by Depleting Intracellular Glutathione Levels. *Angew. Chem. Int. Ed.* **2020**, *59* (20), 7944–7952.

(38) Ahmad, M.; Chattopadhayay, S.; Mondal, D.; Vijayakanth, T.; Talukdar, P. Stimuli-Responsive Anion Transport through Acylhydrazone-Based Synthetic Anionophores. *Org. Lett.* **2021**, *23* (19), 7319–7324.

(39) Chattopadhayay, S.; Wanjari, P.; Talukdar, P. Acylhydrazone-Based Reversibly Photoswitchable Ion Pair Transporter with OFF–ON Cotransport Activity. *Chem. Sci.* **2024**, *15* (41), 17017–17025.

(40) Zhou, Y.; Chen, Y.; Zhu, P.-P.; Si, W.; Hou, J.-L.; Liu, Y. Reversible Photo-Gated Transmembrane Channel Assembled from an Acylhydrazone-Containing Crown Ether Triad. *Chem. Commun.* **2017**, *53* (26), 3681–3684.

(41) Shao, B.; Fu, H.; Aprahamian, I. A Molecular Anion Pump. *Science* **2024**, *385* (6708), 544–549.

(42) Grählert, E.; Langton, M. J. Transmembrane Delivery of an Aryl Azopyrazole Photo-Switchable Ion Transporter Relay. *Angew. Chem. Int. Ed.* **2025**, *64* (6), e202421580.

(43) Johnson, T. G.; Sadeghi-Kelishadi, A.; Langton, M. J. A Photo-Responsive Transmembrane Anion Transporter Relay. *J. Am. Chem. Soc.* **2022**, *144* (23), 10455–10461.

(44) Wezenberg, S. J.; Chen, L.-J.; Bos, J. E.; Feringa, B. L.; Howe, E. N. W.; Wu, X.; Siegler, M. A.; Gale, P. A. Photomodulation of Transmembrane Transport and Potential by Stiff-Stilbene Based Bis(Thio)Ureas. *J. Am. Chem. Soc.* **2022**, *144* (1), 331–338.

(45) Brum, J. de O. C.; França, T. C. C.; LaPlante, S. R.; Villar, J. D. F. Synthesis and Biological Activity of Hydrazones and Derivatives: A Review. *Mini-Rev. Med. Chem.***2020**, *20* (5), 342–368.

(46) Shao, B.; Aprahamian, I. Hydrazones as New Molecular Tools. *Chem* **2020**, *6* (9), 2162–2173.

(47) Murail, S.; Vasiliu, T.; Neamtu, A.; Barboiu, M.; Sterpone, F.; Baaden, M. Water Permeation across Artificial I-Quartet Membrane Channels: From Structure to Disorder. *Faraday Discuss.* **2018**, *209* (0), 125–148.

(48) Kokan, Z.; Chmielewski, M. J. A Photoswitchable Heteroditopic Ion-Pair Receptor. *J. Am. Chem. Soc.* **2018**, *140* (47), 16010–16014.

(49) Vijayvergiya, V.; Wilson, R.; Chorak, A.; Gao, P. F.; Cross, T. A.; Busath, D. D. Proton Conductance of Influenza Virus M2 Protein in Planar Lipid Bilayers. *Biophys. J.* **2004**, *87* (3), 1697–1704.

(50) Akeson, M.; Deamer, D. W. Proton Conductance by the Gramicidin Water Wire. Model for Proton Conductance in the F1F0 ATPases? *Biophys. J.* **1991**, *60* (1), 101–109.

(51) Hunter, C. A.; Anderson, H. L. What Is Cooperativity? *Angew. Chem. Int. Ed.* **2009**, *48* (41), 7488–7499.

(52) Decoursey, T. E. Voltage-Gated Proton Channels and Other Proton Transfer Pathways. *Physiol. Rev.* **2003**, *83* (2), 475–579.

(53) Hu, F.; Luo, W.; Hong, M. Mechanisms of proton conduction and gating in influenza M2 proton channels from solid-state NMR. *Science* 2010, *330*, 505-508.

(54) Brown, L.S. Light-driven proton transfers and proton transport by microbial rhodopsins - A biophysical perspective, *BBA - Biomembranes*, **2022**, *1864*, 183867.

(55) Yan, T.; Liu, S.; Xu, J.; Sun, H.; Yu, S.; Liu, J. Unimolecular Helix-Based Transmembrane Nanochannel with a Smallest Luminal Cavity of 1 Å Expressing High Proton Selectivity and Transport Activity. *Nano Lett.* **2021**, *21*, 10462- 10468.

(56) Andrei, I. M.; Chen, W.; Baaden, M.; Vincent S., Barboiu, M. Proton- versus cation-selective transport of saccharide rim-appended pillar[5]arene artificial water channels, *J. Am. Chem. Soc.* **2023**, *145*, 21904–21914.

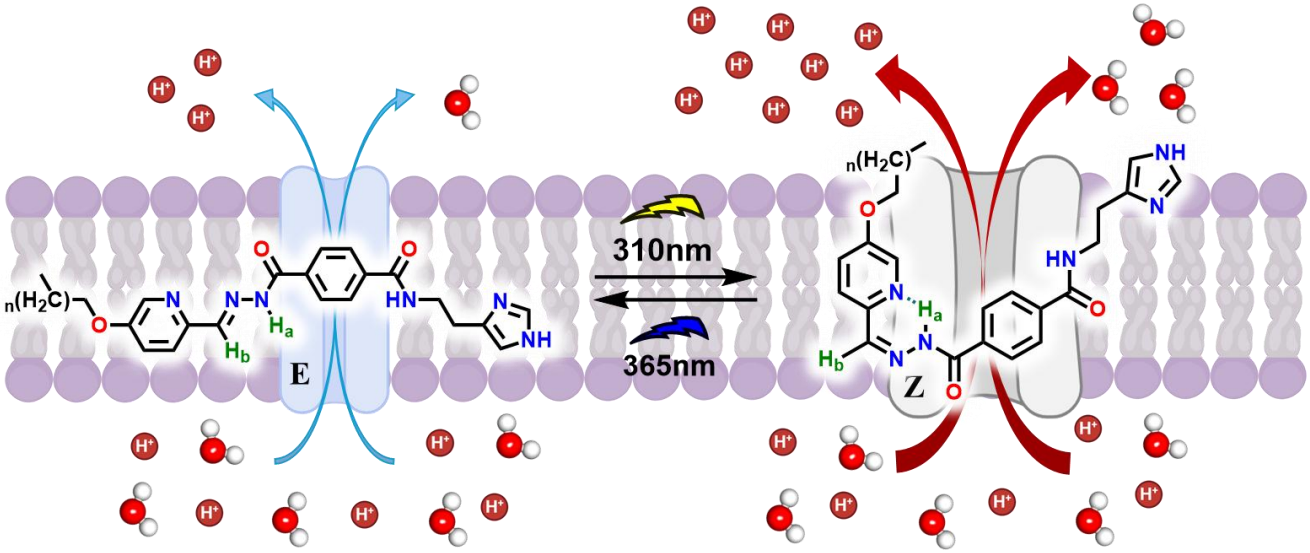

Rigid - Restricted Water/Proton Flow

Dynamic - Increased Water/Proton Flow